VARIABLE-SLOPE REFLECTIVE SURFACES FOR OPTICAL SYSTEM TESTING *VIA* NOVEL DIRECT LASER WRITING-BASED MICROREPLICATION

Declan M. Fitzgerald[1,2], Ryan D. Sochol[1], and Anant Agrawal[2]
[1]University of Maryland, College Park, Maryland, USA
[2]Food and Drug Administration, Silver Spring, Maryland, USA

ABSTRACT

Optical coherence tomography (OCT) is a medical imaging modality that has revolutionized ophthalmology by enabling high-resolution visualization and precise measurements of various ocular structures *in vivo*, particularly within the retina. Despite its widespread use, fundamental engineering parameters (e.g. signal sensitivity) lack standardized evaluation procedures. Here we present a novel way to quantify the signal sensitivity of OCT systems by leveraging "Two-Photon Direct Laser Writing (DLW)"-based additive manufacturing, elastomeric microreplication, and thermally activated selective topographic equilibrium (TASTE) to achieve nonplanar micro/nanostructured devices (or "phantoms") with tailored reflectivity. We investigate the utility of these phantoms for sensitivity quantification using a state-of-the-art laboratory OCT system for retinal imaging. Returned signal intensity, I_{sample}, profiles across multiple microstructures (n = 15) revealed that the sloped surfaces successfully produced both light-abundant and light-starved conditions. Corresponding the effective reflectivity of a region of the microstructure to the returned signal intensity of that region revealed that the minimum sample reflectivity, R_{min}, for which the system could distinguish signal from noise (*i.e.* signal sensitivity) was -61 dB. The phantom's ability to both produce a complete range of signal returns and to precisely determine the R_{min} value of an OCT system suggests its effectiveness as a regulatory tool for OCT sensitivity evaluation.

KEYWORDS

Direct Laser Writing, Two Photon Polymerization, Optical Coherence Tomography

INTRODUCTION

Non-invasive *in vivo* observation of sub-surface human anatomy is an invaluably safe and effective method for disease diagnostics and management. Optical coherence tomography (OCT) stands as one of the gold standard imaging modalities for the human eye, firmly establishing its position in ophthalmic research and medical practices [1,2]. By implementing low-coherence interferometry, OCT can achieve resolutions on the scale of a few microns both axially and laterally [3], enabling OCT use in a variety of ophthalmic applications, including the diagnosis and management of macular degeneration [4,5] and glaucoma [6,7].

As with any medical technology, comprehensive evaluation of OCT imaging devices from laboratory development to clinical implementation is necessary to ensure optimal healthcare outcomes. A frequently-employed physical test object for imaging devices is the phantom, which has carefully established properties for enabling real-world comparisons between an imaging system's output and known, true quantities. They are commonplace in medical imaging, with various types of phantoms developed for other imaging modalities such as magnetic resonance imaging (MRI), computerized tomography (CT), and ultrasound [8-10].

The signal-to-noise ratio (SNR) is a fundamental measure of OCT system sensitivity, relating signal intensity to noise variance, and is defined as:

$$\mathrm{SNR} = \frac{I_{sample}^2}{\sigma_{background}^2} \qquad (1)$$

Where I_{sample} is the signal intensity from the sample and $\sigma_{background}^2$ is the noise variance. SNR is usually reported in decibels, as:

$$\mathrm{SNR[dB]} = 10 \times \log_{10}(\mathrm{SNR}) \qquad (2)$$

Sensitivity is a commonly referenced performance metric that denotes a system's ability to discern between signal and noise in light-starved conditions, as frequently occurs during tissue imaging, and is defined as the minimum sample reflectivity, R_{min}, for which SNR = 0 dB [11]. Despite its importance, sensitivity lacks any formal evaluation technique. In our previous work we also noted that the traditional method for evaluating system sensitivity is limited by an assumed linear relationship between performance in light-abundant and light-starved conditions [12]. In this paper, we present a new approach for OCT sensitivity measurement that directly evaluates the minimum detectable signal strength. To that end, we developed a phantom with angled 3D microstructures that vary the amount of light returned to the imaging system down to and below the minimum detectable signal level and demonstrated its use with a cutting-edge retinal imaging OCT system.

CONCEPT

The concept behind the microstructured sensitivity phantom is that by varying the effective reflectivity across the microstructure *via* slope angle modulation, the location where SNR = 0 dB can be directly traced to an R_{min} value. By including a range of slope angles, each microstructure can include regions from complete light

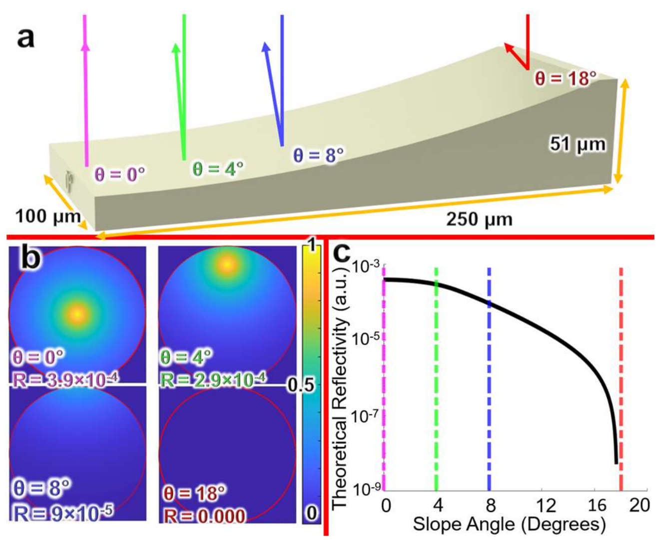

Figure 1: Conceptual demonstration of slope angle-modulated theoretical reflectivity, and theoretical results of ray-tracing simulation. a) Microstructure dimensions and individual beam interactions at different slope angles. b) Intensity profiles of light returned to detector for respective slope angles. c) Theoretical reflectivity curve for range of angles included in microstructure, calculated for OCT system used in this study.

978-1-940470-05-4/HH2024/$25©2024TRF
DOI 10.31438/TRF.HH2024.118

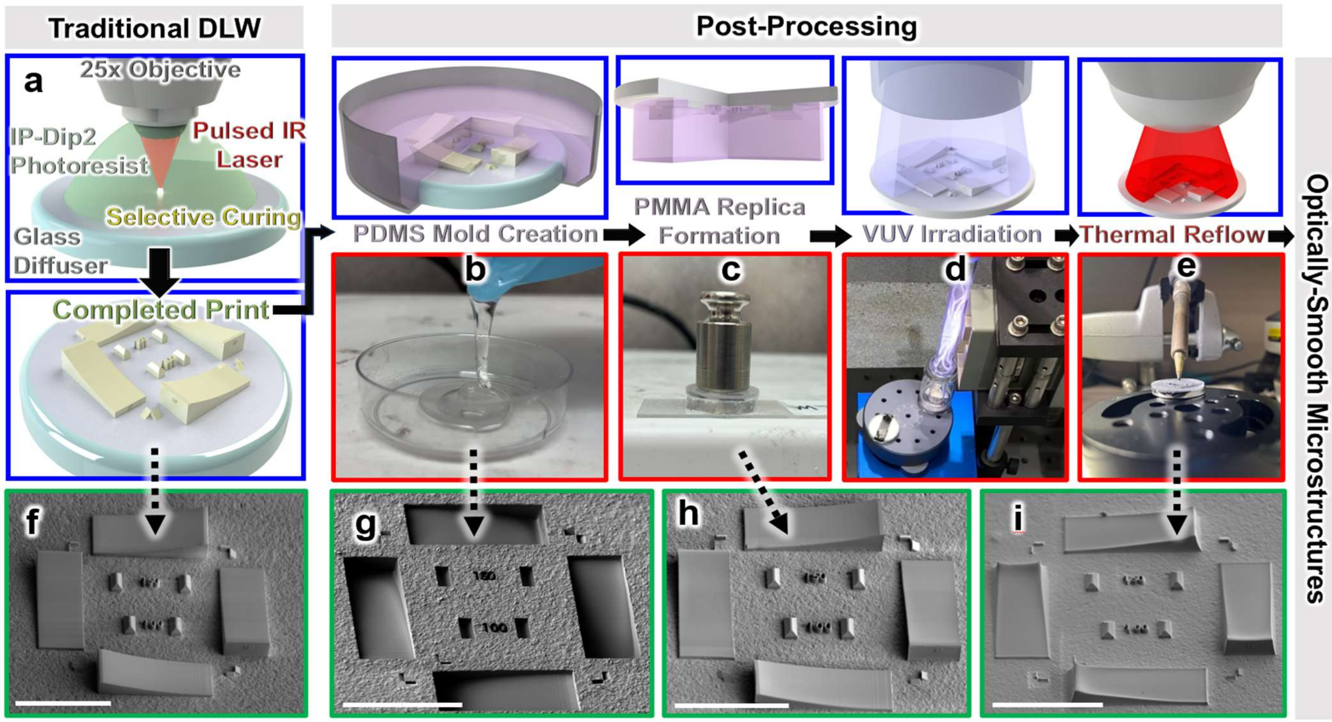

Figure 2: Direct Laser Writing (DLW)-enabled microstructures with variable-sloped surfaces for optical coherence tomography (OCT) sensitivity analysis. CAD renderings framed in blue, photographs framed in red, SEM images framed in green. a) DLW-printing onto a glass diffuser. b) PDMS negative mold fabrication with DLW print. c) Molding of PMMA/Anisole solution and weighted curing to PMMA substrate. d) Vacuum UV-dosing of superficial layer of PMMA sample. e) Thermal dosing using mounted soldering iron. SEM images of f) a DLW printed phantom, g) a PDMS negative mold, h) a PMMA replica, and i) a VUV and thermally-dosed phantom. Scale bars = 250 µm.

return to no return at all, ensuring that R_{min} is present somewhere along the curve (Fig. 1). The baseline reflectivity is determined by the refractive index mismatch between the PMMA/air interface at the phantom surface and the 1.0 OD attenuating filter used to prevent saturation. The theoretical reflectivity curve is calculated via a ray-tracing simulation where local microstructure angle determines incident light percentage returned to the detector, with a Gaussian beam illumination with $1/e^2$ diameter of 6.7 mm.

MATERIALS AND METHODS

Direct Laser Writing (DLW)

The microstructures are printed with the Nanoscribe Photonic Professional GT2 DLW 3D printer (Nanoscribe, Karlsruhe, Germany) with a 25× objective (Fig. 2a). Slicing and hatching parameters are set to 100 nm. The printing material is Nanoscribe's proprietary IP-Dip2 resin on a silanized glass diffuser with a 1200-grit sandblasted surface (DG1200, Thorlabs, Newton, NJ). The print is then soaked in a propylene glycol methyl ether acetate (PGMEA) bath for 15 minutes, followed by an isopropyl alcohol (IPA) bath for 5 minutes, and finally placed in a UV cure box for 10 minutes. A complete print is shown in Figure 2f.

PMMA Replication

The glass diffuser is placed print side up in a plastic petri dish and covered with polydimethylsiloxane (PDMS) elastomer (Sylgard 182, Dow Corning) and cured for 6 hours on a hotplate at 65°C, creating a PDMS negative of the phantom (Fig. 2b). The PDMS negative is then placed on a hot plate at 65°C, and 30 μL of 5:1 anisole and 120k PMMA solution is placed on the surface of the PDMS. This is left for 5 minutes to purge any bubbles. A 25-mm diameter PMMA disk is then placed on top of the PDMS negative and secured with a 35 g weight, remaining on the hotplate for another 20 minutes (Fig. 2c). The PMMA disk is peeled away from the PDMS negative, taking the newly-cured PMMA film with it.

Thermally activated selective topographic equilibrium (TASTE)

The surface texture resulting from DLW's layer-by-layer curing process prevents the microstructures from acting as perfect reflectors. Previous work has demonstrated thermally activated selective topographic equilibrium (TASTE), a process utilizing a positive-tone photoresist and depth-controlled softening to smooth the surface roughness resulting from different lithographic techniques [13]. TASTE was successfully implemented by Chidambaram et al. in the smoothing of microstructures originally fabricated via DLW and transferred into PMMA [14]. As demonstrated by Helmut Schift's research group, PMMA's positive-tone resist behavior can be isolated to a superficial μm-thick layer *via* exposure to vacuum-UV (VUV) radiation. This allows for a targeted softening of the surface texture while leaving the underlying structural PMMA unchanged.

A VUV xenon lamp (LC-X, Opthos Instrument Company, Maryland, USA) centered at a wavelength of λ = 172 nm is used to irradiate the PMMA film (Fig. 2d). Each PMMA sample is exposed to a total VUV dose of 1.46 J cm^{-2}, with an estimated 50% absorbed within the first micron of the PMMA film. A mounted soldering iron is then used to heat the surface of the substrate containing the microstructure array (Fig. 2e). A thermocouple is used to confirm PMMA surface temperature. A surface temperature of 87±1.5°C is maintained for 2.5 minutes to complete the reflow process.

Phantom Evaluation

SEM micrographs (Mira 3, TESCAN, Brno, Czech Republic)

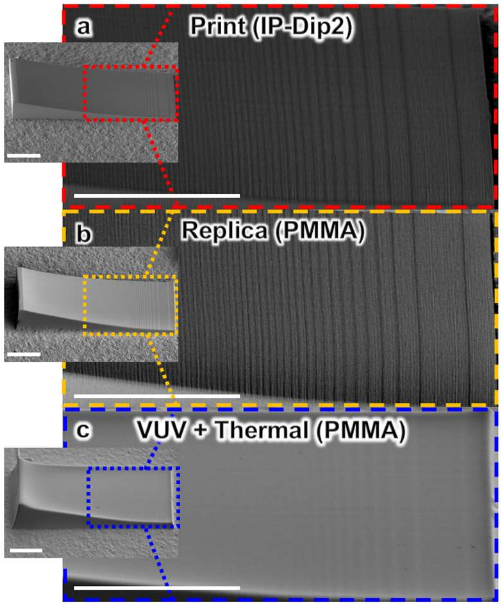

Figure 3: Two SEM perspectives of a single sloped microstructure from a) the DLW printed phantom, b) a PMMA replica molded from the PDMS negative, and c) a PMMA replica after VUV and thermal exposures. Scale bars = 50 µm.

were taken of 5 nm gold-coated samples to provide high-resolution images of the phantom at every stage of its development. Stylus profilometry (Dektak 150, Veeco, New York, USA) was performed to determine true slope angles. Brightfield microscopy (Optiphot, Nikon, Tokyo, Japan) was used to confirm scale bar separation post-reflow, which was then used to establish scale within each OCT image. The primary OCT device used in this work is an ophthalmic spectral-domain adaptive optics (AO)-enhanced OCT system constructed at the FDA [15]. The OCT evaluation serves two purposes: 1) to assess the change in microstructure reflectivity that results from the post-processing, and 2) to assess the phantom's ability to determine an OCT system's minimum reflectivity threshold.

RESULTS AND DISCUSSION

PMMA Replication and TASTE

The elastomeric micromolding technique produced faithful replicas of the original DLW print, accurately recreating both macroscopic structural features and sub-micrometer features such as individual slicing layers (Fig. 3a-b). Over the course of this investigation, more than 100 PMMA replicas of various designs have been created using this approach, exhibiting high repeatability and resolution.

SEM micrographs provided visual evidence that the TASTE process was effective in its reduction of the surface texture resulting from the DLW print process. The prominent stair-like features seen in both the DLW print and the PMMA replica become less obtrusive on the phantom after VUV and thermal treatment (Fig. 3).

Change in Surface Reflectivity

The SNR between the print and the processed phantoms is not significantly different for slope angles less than 12° ($p > 0.05$, $n = 44$) but is significantly lower from the processed phantom for slope angles greater than 12° ($p < 0.001$, $n = 182$). A significantly lower SNR at higher slope angles indicates that the microstructure's surface has become more optically smooth, allowing it to reflect the majority of the incident beam away from the detector as intended.

The surface roughness inherent to the DLW process limits the optical performance of the print, as anticipated by previous works [16]. The stair-like geometry allows the local flat spots of each individually printed layer to reflect light back to the detector, despite the intended slope of the region (Fig. 4b). The processed phantom had these flat spots reflowed into a continuous curve, successfully preventing the return of light in higher-sloped regions (Fig. 5b).

OCT Sensitivity

In order for the phantom to directly quantify the OCT minimum detectable reflectivity threshold, it must both 1) achieve surface conditions for which the system's SNR = 0 dB, and 2) allow for accurate estimation of the effective reflectivity of the microstructure at the location where this condition is achieved. The phantom reaches the SNR = 0 dB threshold across multiple samples in a repeatable manner (Fig. 5c). By using profilometry to confirm precise surface slope angles, the phantom's effective reflectivity can be quantified across its entire surface. By taking the average slope angle of the datapoints closest to the SNR = 0 dB threshold and determining the effective reflectance at that slope angle, we can determine the OCT system's sensitivity. With an average zero-return angle of 16.67°, we find $R_{min} = 7.28\times10^{-7}$, or -61 dB.

The traditional method of OCT sensitivity evaluation uses the maximum SNR a device can achieve, SNR_{max}, determined by imaging a highly reflective surface to maximize I_{sample}. Just as the minimally-reflective sloped regions of the microstructures allow for direct calculation of R_{min}, the highly reflective flat regions enable a direct calculation of SNR_{max}. This allows for a direct comparison of sensitivity assessment methods. By averaging the SNR value of the datapoints closest to a slope angle of zero and using equation 4 from Agrawal et. al. [12], we found SNR_{max} = 93 dB, higher than Liu et. al. reported for the same system, a difference we have yet to reconcile [15]. The SNR_{max} result from our phantom is also 32 dB higher than the sensitivity determined via direct estimation of R_{min}. This result is consistent with previous work by our group, in which microsphere suspensions of known reflectivity were also used to

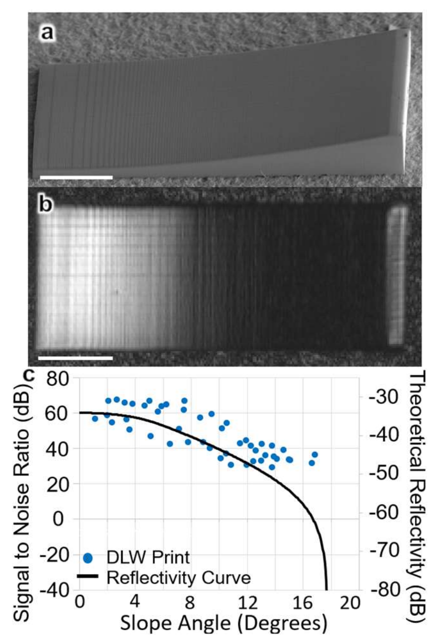

Figure 4: a) SEM and b) AOOCT images of a single DLW printed angled microstructure with slope increasing from left to right. Scale bars = 50 µm. c) Signal to noise ratio plotted against slope for the DLW printed phantom. The theoretical reflectivity versus slope angle profile for the AOOCT system is overlaid on c).

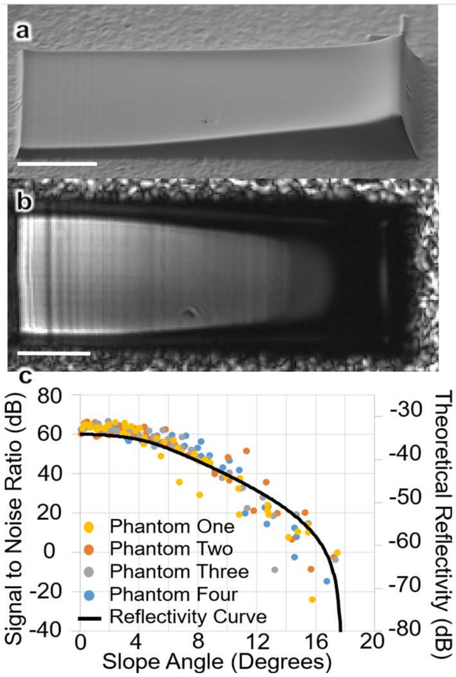

Figure 5: a) SEM and b) AOOCT images of a single fully-processed angled microstructure with slope increasing from left to right. Scale bars = 50 µm. c) Signal to noise ratio plotted against slope for the fully processed phantoms. The theoretical reflectivity versus slope angle profile for the AOOCT system is overlaid on c).

directly calculate R_{min}, finding that it undershot the traditional SNR_{max} evaluation by 26 dB [12]. The previous and current results highlight the fact that any assumed linear relationship between OCT system performance in light-abundant (i.e., under a shot noise-limited condition) and light-starved conditions is not valid, and that the widely-used sensitivity analysis procedure overestimates system performance.

CONCLUSIONS

An optical phantom for direct OCT sensitivity evaluation has been developed by combining the geometric versatility of DLW and the selective surface smoothing of TASTE. Each microstructure within the phantom successfully produced both light-abundant and light-starved regions with known effective reflectivity. The phantom's solid-state composition, continuous range of reflectivities, and easily-replicated nature are critical features that improve stability and accessibility for OCT system development, deployment, maintenance, and standardization. The OCT phantom will enable more rigorous and verifiable evaluation of OCT system sensitivity. Future work will better characterize the structural changes resulting from the TASTE process. These results demonstrate that the phantom is an effective regulatory tool for OCT sensitivity evaluation.

ACKNOWLEDGEMENTS

This research was supported in part by U.S. National Science Foundation (NSF) Award #1943356. Declan M. Fitzgerald was supported by the Oak Ridge Institute for Science and Engineering (ORISE) fellowship program at the FDA.

DISCLAIMER

The mention of commercial products, their sources, or their use in connection with material reported herein is not to be construed as either an actual or implied endorsement of such products by the U.S. Department of Health and Human Services.

REFERENCES

[1] R. Chopra, S. K. Wagner, and P. A. Keane, "Optical coherence tomography in the 2020s—outside the eye clinic," *Eye* 35 (2021), pp. 236–243.

[2] E. A. Swanson and J. G. Fujimoto, "The ecosystem that powered the translation of OCT from fundamental research to clinical and commercial impact [Invited]," *Biomed Opt Express*, vol. 8, no. 3 (2017), p. 1638.

[3] D. R. Williams, "Imaging single cells in the living retina," *Vision Research*, vol. 51, no. 13 (2011), pp. 1379–1396.

[4] P. A. Keane, P. J. Patel, S. Liakopoulos, F. M. Heussen, S. R. Sadda, and A. Tufail, "Evaluation of Age-related Macular Degeneration With Optical Coherence Tomography," *Survey of Ophthalmology*, vol. 57, no. 5 (2012), pp. 389–414.

[5] L. de Sisternes, N. Simon, R. Tibshirani, T. Leng, and D. L. Rubin, "Quantitative SD-OCT imaging biomarkers as indicators of age-related macular degeneration progression," *Invest Ophthalmol Vis Sci*, vol. 55, no. 11 (2014), pp. 7093–7103.

[6] WuDunn D, Takusagawa HL, Sit AJ, Rosdahl JA, Radhakrishnan S, Hoguet A, Han Y, Chen TC., "OCT Angiography for the Diagnosis of Glaucoma: A Report by the American Academy of Ophthalmology," *Ophthalmology*, vol. 128, no. 8 (2021), pp. 1222–1235.

[7] D. S. Grewal and A. P. Tanna, "Diagnosis of glaucoma and detection of glaucoma progression using spectral domain optical coherence tomography," *Current Opinion in Ophthalmology*, vol. 24, no. 2 (2013), pp. 150–161.

[8] E. Villa, N. Arteaga-Marrero, J. González-Fernández, and J. Ruiz-Alzola, "Bimodal microwave and ultrasound phantoms for non-invasive clinical imaging," *Sci Rep*, vol. 10, no. 1 (2020).

[9] A. Valladares, T. Beyer, and I. Rausch, "Physical imaging phantoms for simulation of tumor heterogeneity in PET, CT, and MRI: An overview of existing designs," *Medical Physics*, vol. 47, no. 4 (2020), pp. 2023–2037.

[10] K. E. Keenan *et al.*, "Quantitative magnetic resonance imaging phantoms: A review and the need for a system phantom," *Magnetic Resonance in Medicine*, vol. 79, no. 1 (2018), pp. 48–61.

[11] J. F. de Boer, R. Leitgeb, and M. Wojtkowski, "Twenty-five years of optical coherence tomography: the paradigm shift in sensitivity and speed provided by Fourier domain OCT [Invited]," *Biomed Opt Express*, vol. 8, no. 7 (2017), p. 3248.

[12] A. Agrawal, T. J. Pfefer, P. D. Woolliams, P. H. Tomlins, and G. Nehmetallah, "Methods to assess sensitivity of optical coherence tomography systems," *Biomed Opt Express*, vol. 8, no. 2 (2017), pp. 902-917.

[13] A. Schleunitz, V. A. Guzenko, M. Messerschmidt, H. Atasoy, R. Kirchner, and H. Schift, "Novel 3D micro- and nanofabrication method using thermally activated selective topography equilibration (TASTE) of polymers," *Nano Converg*, vol. 1, no. 1 (2014).

[14] N. Chidambaram, R. Kirchner, R. Fallica, L. Yu, M. Altana, and H. Schift, "Selective Surface Smoothening of Polymer Microlenses by Depth Confined Softening," *Adv Mater Technol*, vol. 2, no. 5, (2017).

[15] Z. Liu, J. Tam, O. Saeedi, and D. X. Hammer, "Trans-retinal cellular imaging with multimodal adaptive optics," Biomed. Opt. Express 9 (2018), pp. 4246-4262

[16] K. Takada, H.-B. Sun, and S. Kawata, "Improved spatial resolution and surface roughness in photopolymerization-based laser nanowriting," *Appl Phys Lett*, vol. 86, no. 7 (2005), p. 071122.

CONTACT

* R. D. Sochol, tel: 1+ (301) 405-6928; rsochol@umd.edu